H2020-FETFLAG-2018-2021

macQsimal

Miniature Atomic vapor-Cell Quantum devices for SensIng and Metrology AppLications

Deliverable D8.3

Quantification of bandwidth and sensitivity of NO sensor

WP8 - Rydberg gas sensors

Authors: Robert Löw, Harald Kübler, Fabian Munkes, Patrick Kaspar, Tilman Pfau (STUTT)

Lead participant: STUTT

Delivery date: 11.07.2022

Dissemination level: Public

Type: R (Document, Report)

This work has received funding from the European Union's Horizon 2020 research and innovation programme under grant agreement No. 820393.

Revision History

Author Name, Partner short name	Description	Date
Robert Löw (STUTT), Harald Kübler (STUTT), Fabian Munkes (STUTT), Patrick Kaspar (STUTT), Tilman Pfau (STUTT)	Draft deliverable	23.06.2022
Janine Riedrich-Möller (BOSCH)	Revision 1	27.06.2022
Robert Löw (STUTT)	Final version	11.07.2022
Johannes Ripperger (accelCH)	Final formal checks and formatting	11.07.2022

Contents

1 INTRODUCTION 5

2 GAS GLASS CELL 5

2.1 Measurement procedure 6

2.2 Analysis of spectroscopic lines 7

2.2.1 Transitions 7

2.3 Optimal sensing regime 8

2.4 Bandwidth and sensitivity 9

Abbreviations and short names of macQsimal project partners

accelCH	accelopment Schweiz AG, CH
BOSCH	Robert Bosch GmbH, DE
NO	Nitric oxide
PCB	Printed circuit board
STUTT	Universität Stuttgart, DE
TIA	Trans-impedance amplifier
UV	Ultraviolet
WP	Work Package

Executive Summary

This deliverable is dedicated to estimate the achievable sensitivity of our envisioned NO-trace gas sensor. The estimates made here are based on our previous work on the Rubidium-trace gas sensor (see deliverable D8.2), the Rydberg spectroscopy (see deliverable D8.1) and our recent spectroscopic studies with respect to pressure broadening and saturation broadening. Besides this we included our experimental results on our custom-made trans-impedance amplifiers and the foreseen potential of these amplifiers. The optimal performance is taking place in a ballistic regime for the gas-molecules. Therefore, the optimal size of the detector is mostly dominated by the size of the laser beams and the conductivity of the through-flow cell.

1 Introduction

This report focuses on the optimization of the Rydberg gas-sensor prototype for nitric oxide (NO). In the first part a new glass cell is introduced. The cell features an on-board trans-impedance amplifier (TIA) which is located on a PCB directly glued to the cell. This allows a significant increase of the signal-to-noise ratio. Exemplary signals are shown for all three transitions. In the second part the parameters which influence the current signal are systematically investigated. These are current, laser power and cell pressure. The investigation allows it to choose optimal values for the sensor prototype. In the last section the dynamical behaviour of the system with regard to chopping frequencies of the green laser is investigated theoretically. This is an important step to later determine time constants for the employment of a lock-in amplifier when further optimization of the detection scheme will be performed.

2 Gas glass cell

In comparison to deliverable D8.1 the detection cell has been greatly improved resulting in an improved sensitivity of the trace-gas sensor.

In contrast to the previous cell the glass cell is considerably smaller now with a light travel path of 2 cm and an electrode distance of 2 cm. The electrodes itself are part of a custom-made PCB glued to a borosilicate glass frame as seen in Figure 1. There is no electrode configuration within the cell, but this might be an addition in the future. As mentioned, the glass frame and tubes are made from borosilicate. The excitation “cage” is open on top, bottom, front and back, to glue the electrodes as well as quartz windows for the laser light to it. Quartz windows are needed because of the UV wavelength of the ground state transition.

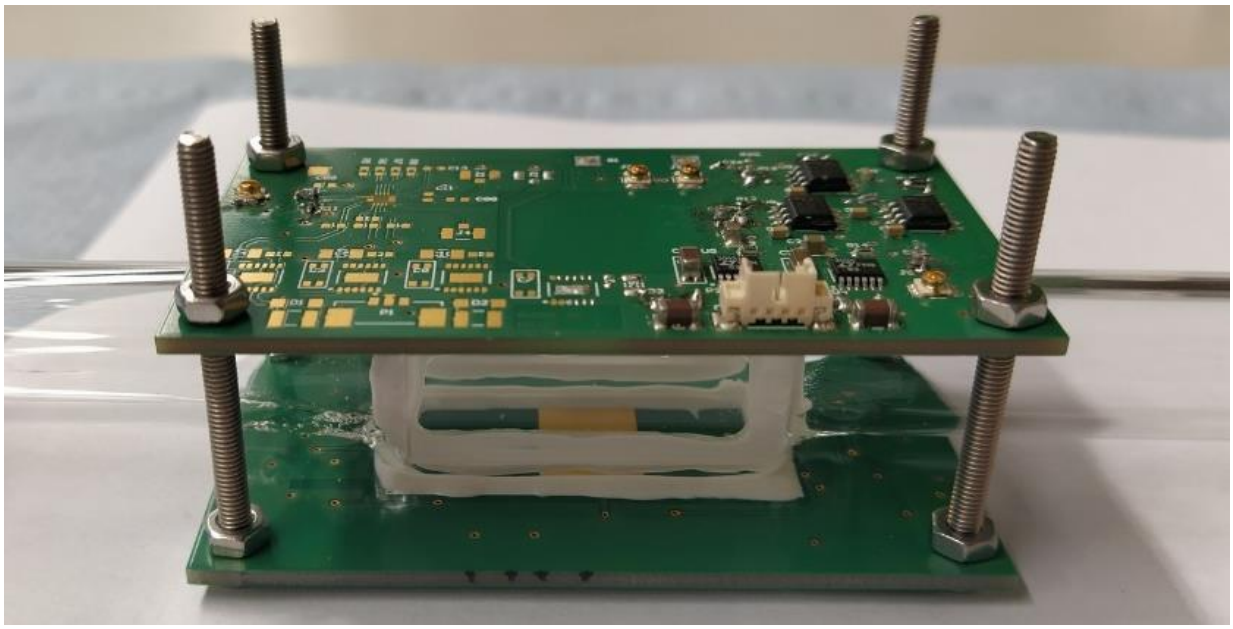

***Figure 1**. Close-up photo of the new electronic cell type. Due to the UV wavelength quartz cell windows are needed. Those are glued to the borosilicate glass cell. The PCBs are glued to the cell as well.*

The custom-made PCB holding the circuit shown in Figure 1 is explained in the respective caption.

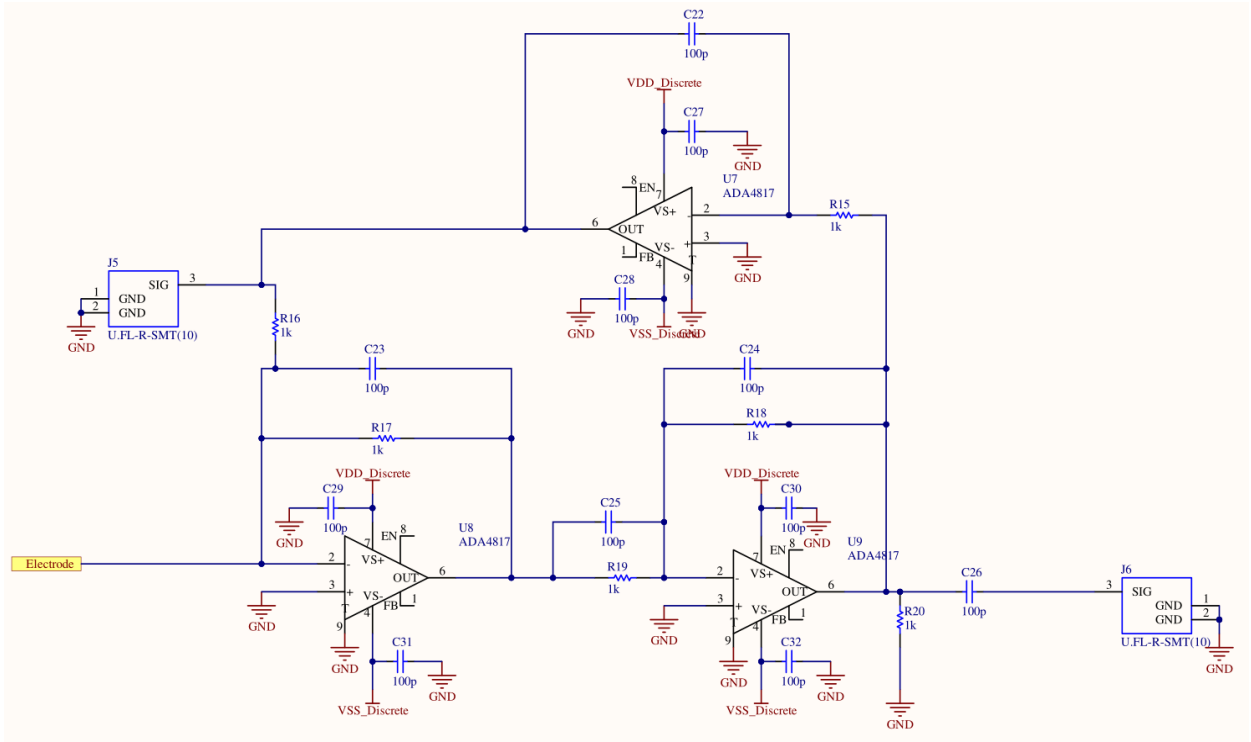

***Figure 2**. Sketch of the discrete amplification circuit. The input signal are the electrons collected at the electrode. The operational amplifiers used are ADA4817.*

Figure 3 shows a picture of the new cell within the setup. Not visible are the power supplies needed.

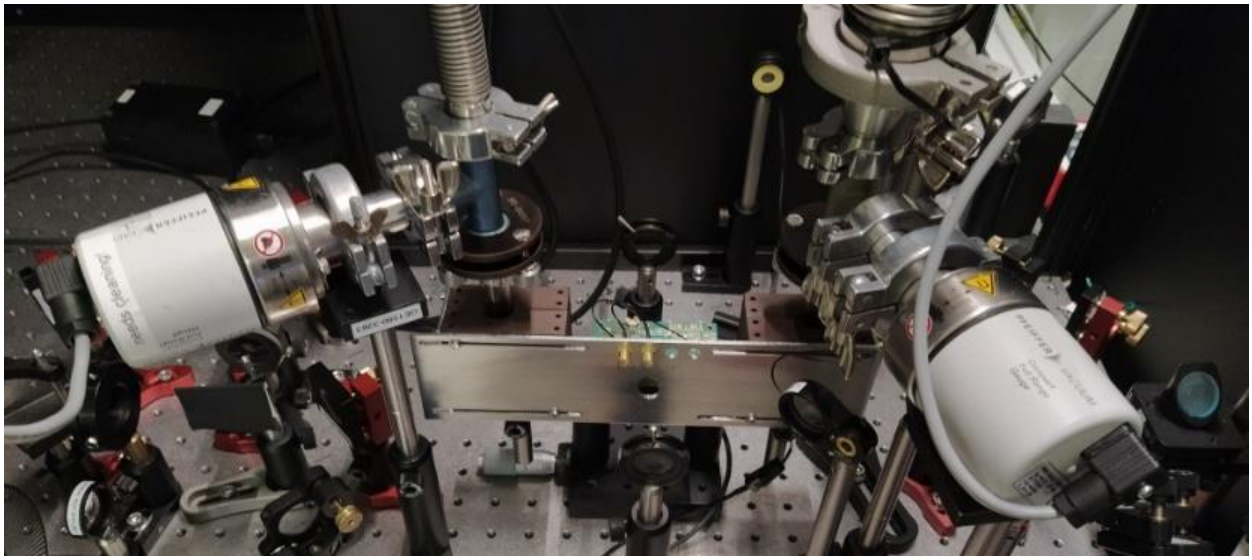

***Figure 3.** Picture of the new cell within the experimental setup. The gas is flowing from left to right. The metal shield allows for easy connection of the readout plugs.*

2.1 Measurement procedure

A small potential difference is applied to the bottom and top electrode to guide free electrons to the electrodes. All measurements presented in this deliverable are taken in single-shot mode, i.e., no averaging or data post-processing was applied. This is in every way superior to the previous cell.

2.2 Analysis of spectroscopic lines

The 3-photon excitation has been introduced in deliverable D8.1. The analysis of the spectroscopic lines presented back then shall be reiterated here using the new cell. All measurements were acquired using the electronic readout.

2.2.1 Transitions

Figure 4 shows an example trace for the ground state transition (226 nm) A 2Σ+ ← X 2Π3/2, P12(5.5) in nitric oxide. An electrical signal can already be observed for the first transition of the three-photon excitation scheme of the targeted trace-gas sensor which is attributed to a two-photon process. This is unfavourable for the sensor, as the selectivity drops if those noise electrons are detected alongside the ones of the Rydberg ionization. The next section shows an overview where better parameters are found.

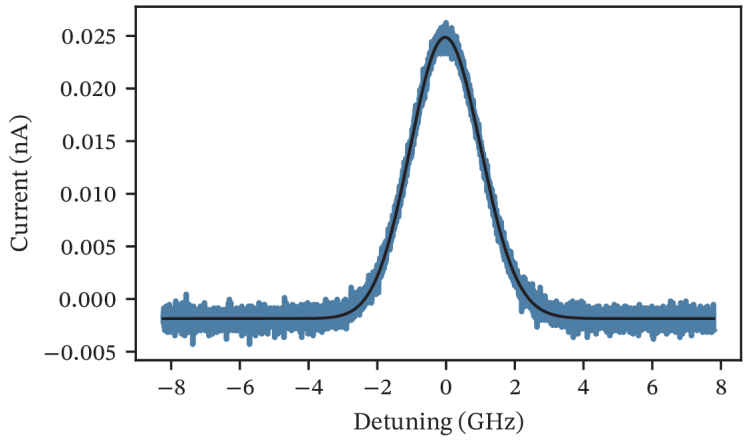

Figure 4. *Example trace of the UV transition's current signal if the laser's frequency is swept (detuning in GHz). The pressure has been 0.112mbar, the beam's power was 14mW.*

The same holds true for the second transition at 540 nm, H 2Σ+← A 2Σ+R11 (4.5) as shown in Figure 5. On the other hand, the ability to detect these transitions might allow for better excitation paths in the future. As already stated in deliverable D8.1 the intermediate transition can only be detected electrically. When compared to Figure 6 in deliverable D8.1 the improvements in noise reduction are obvious even by eye. Despite the current being considerably lower the overall fluctuation of the signal remains low.

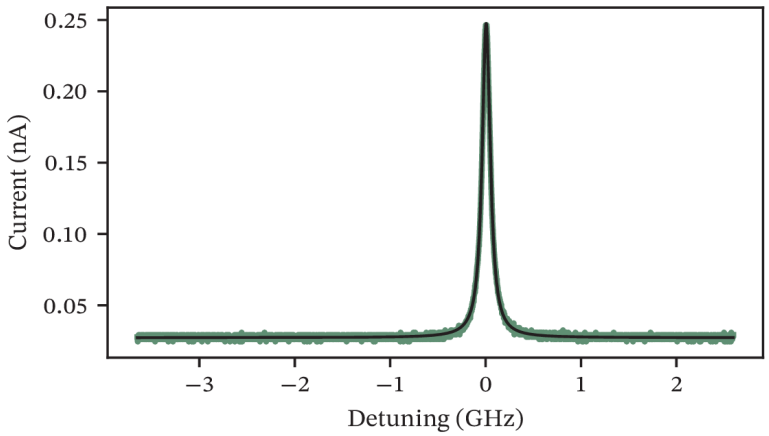

Figure 5. *Example trace of the current signal of the green transition. The pressure has been 0.112 mbar, the UV power was 14 mW, the green power 906 mW. For this measurement, the UV laser was kept constant in frequency at the ground state transition. The green laser was swept in frequency and its detuning is plotted in GHz.*

The final transition is the Rydberg transition at a wavelength of 835 nm. This allows to excite to a Rydberg state "$\Sigma\leftarrow \{H\}\ ^\ \{\ 2\}\ \{\Sigma\ \}\ ^\ \{+\ \Sigma\leftarrow H^2\Sigma^+,,\}$, which is a Σ state. As at this point the exact Rydberg state is not known, we are not able to assign a principle quantum number.

Figure 6 shows an exemplary Rydberg signal. Again, the improvements when compared to deliverable D8.1 are obvious. Several peaks are visible as the noise was greatly reduced.

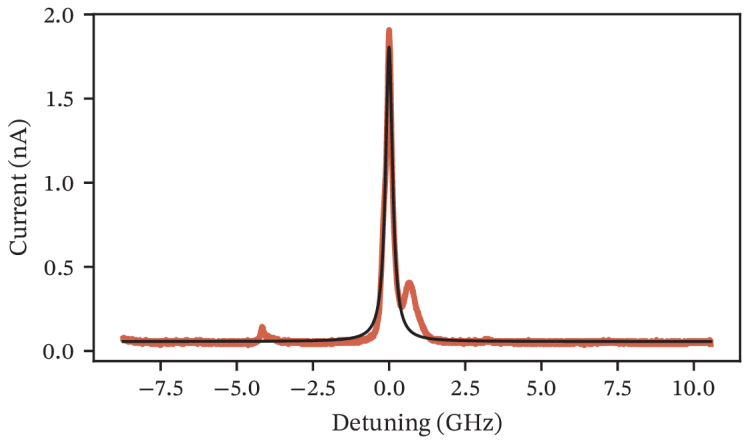

Figure 6. *Current signal of the Rydberg transition exemplary shown for a power of 260 mW of the Rydberg laser, 900 mW for the green laser and 14 mW for the UV laser. The pressure was 0.113 mbar. The Rydberg laser was swept in frequency and its detuning is shown. The other two lasers were kept at the frequency of their respective transition.*

2.3 Optimal sensing regime

Figure 7 gives an overview for changes in power, voltage or pressure. The used transitions are A $^2\Sigma^+ \leftarrow$ X $^2\Pi_{3/2}$, $P_{12}(5.5)$ for the first (UV) transition H $^2\Sigma^+\leftarrow$ A $^2\Sigma^+R_{11}(4.5)$ for the intermediate (green) transition and finally the last (red) transition to some Rydberg state "$\Sigma\leftarrow \{H\}\ ^\ \{\ 2\}\ \{\Sigma\ \}\ ^\ \{+\}\ .\Sigma\leftarrow H^2\Sigma^+$. For all subplots the maximum current of a specific measurement, as seen previously, is plotted. For a power sweep, voltage and pressure are kept constant. For a voltage sweep power and pressure are kept constant. Finally, for a pressure sweep power and voltage are kept constant.

For the power sweep, the UV transition shows quadratic behaviour, whereas the intermediate and Rydberg transition are considered linear. The quadratic behaviour of the UV transition indicates a two-photon process is at play. The orange bars indicate well-suited measurement parameters for the trace-gas sensor. In terms of power, they are set at 14mW for the UV, at 900 mW for the green and at 260mW for the red transition.

Equally, the voltage sweep can be analysed. For UV and green, the linear behaviour turns into saturation as soon as all free charges are detected. For the Rydberg transition however, the overall current decreases due to an increase in peak width. An optimal voltage, as indicated in orange, appears to be 3 V.

Finally, for all wavelengths the same behaviour for the pressure sweep can be seen. This is easily explained, as for higher pressures the probability of collisions with other particles increases. A low pressure at 0.11 mbar is optimal.

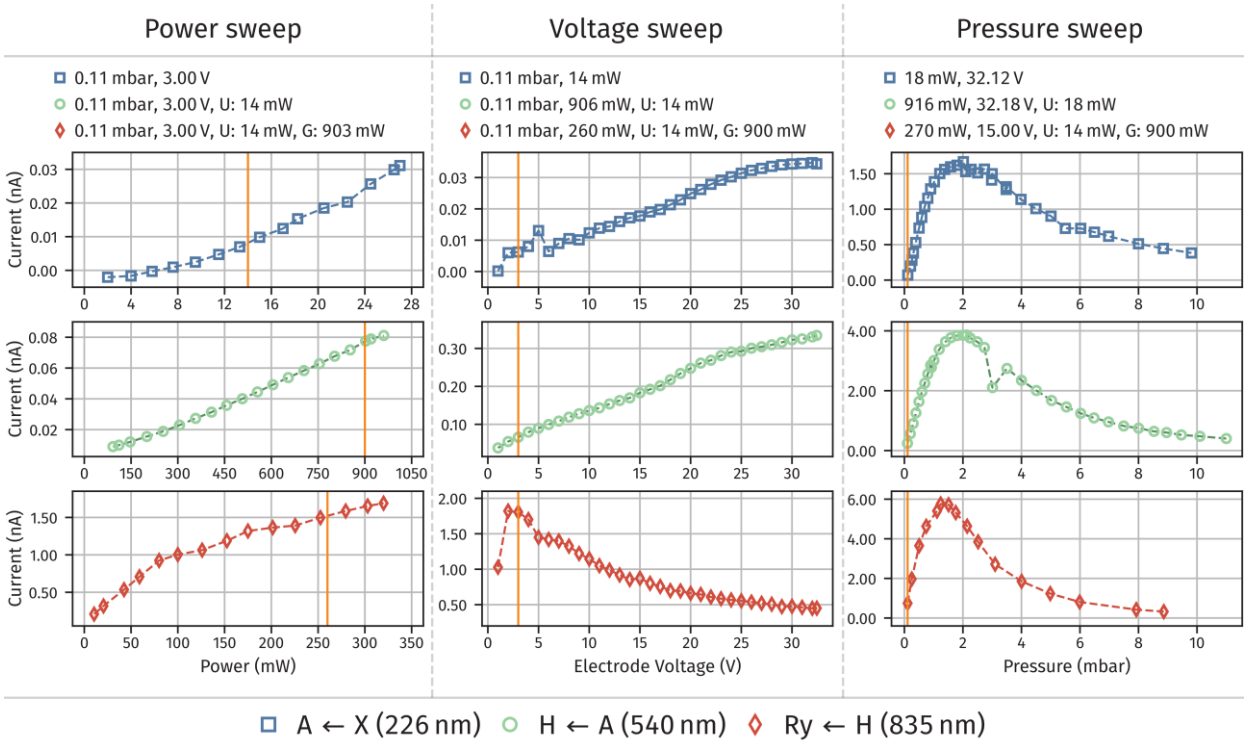

Figure 7. *Overview plot putting all three transitions and their behaviour into perspective. For the UV transition the red and green laser are switched off and the UV frequency is changed. For the green transition the UV laser frequency is kept constant, and the green laser is changed in frequency. Finally, for the red transition the blue and green laser are kept at their respective transition frequency and the red laser's frequency is changed. For all measurements a full trace at their according transition is taken. The plot then shows the maximum current measurement for either a specific power, voltage or pressure. If i.e., the power is changed, the voltage and pressure are kept constant.*

2.4 Bandwidth and sensitivity

To evaluate the currently achievable detection bandwidth and sensitivity, the laser excitation dynamics were simulated using optical Bloch equations. The collisional ionization of excited Rydberg states was modelled using an effective decay rate from the Rydberg state to the ion state. Additionally, transition as well as Doppler broadening were taken into account.

Dynamical constants e.g., dipole moments, that could not be found in literature have been estimated such that the Rabi frequencies approximately match the decay rates. They are in the MHz range. This way power broadening effects are prevalent.

The simulation results are shown in Figure 8. It can be seen that for larger chop frequencies the ion-population drops rapidly at a certain point from an almost constant high to a constant low. The simulation illustrates how crucial the choice of time constants for chopping frequencies and lock-in amplifiers will be when the system is further optimized.

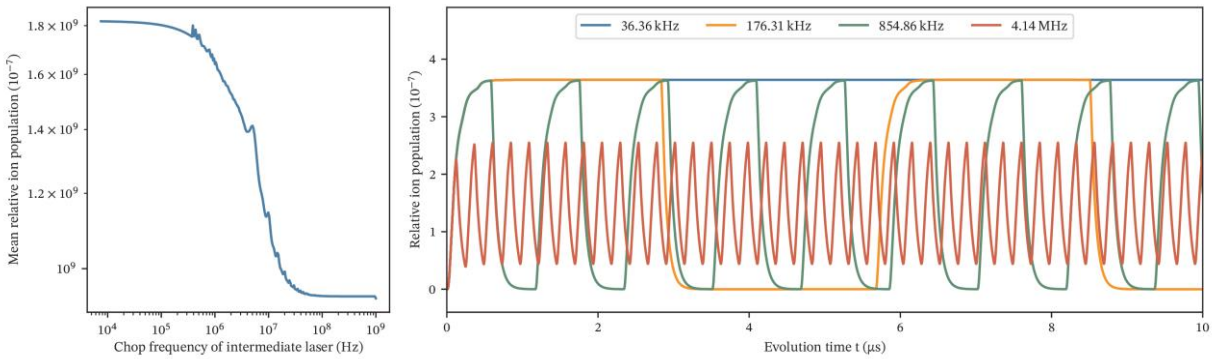

***Figure 8**. On the left subplot the mean ion population is plotted versus the chop frequency of the green laser. On the right-hand side some of the corresponding traces are plotted. Each data point in the left figure corresponds to a trace on the right side.*